

PAPER • OPEN ACCESS

Structural and dynamic properties of short-period GaN/AlN superlattices grown by submonolayer digital epitaxy

To cite this article: V Yu Davydov *et al* 2020 *J. Phys.: Conf. Ser.* **1697** 012155

View the [article online](#) for updates and enhancements.

You may also like

- [Reducing Kapitza resistance between graphene/water interface via interfacial superlattice structure](#)
Xiaoyi Peng, Pengfei Jiang, Yulou Ouyang et al.
- [Elastic-relaxation-induced barrier layer thickness undulations in InP/GaAs type-II quantum well superlattice structures](#)
S D Singh, Ravi Kumar, C Mukherjee et al.
- [Monochromatic terahertz acoustic phonon emission from piezoelectric superlattices](#)
B A Glavin, V A Kochelap, T L Linnik et al.



ECS
The
Electrochemical
Society
Advancing solid state &
electrochemical science & technology

DISCOVER
how sustainability
intersects with
electrochemistry & solid
state science research

Structural and dynamic properties of short-period GaN/AlN superlattices grown by submonolayer digital epitaxy

V Yu Davydov¹, E M Roginskii¹, Yu E Kitaev¹, A N Smirnov¹, I A Eliseyev¹,
M A Yagovkina¹, D V Nechaev¹, V N Jmerik¹ and M B Smirnov²

¹Ioffe Institute, 26 Politekhnicheskaya, St. Petersburg, 194021, Russia

²Saint-Petersburg State University, St. Petersburg, 194508, Russia

E-mail: valery.davydov@mail.ioffe.ru

Abstract. Structural and dynamic properties of short-period GaN/AlN superlattices with the thicknesses of the constituent layers varying from two to several monolayers, grown using the method of submonolayer digital molecular beam epitaxy, are experimentally and theoretically studied. It is established that in the grown samples there are two types of periodicity. One type is formed by periodic sequence of GaN and AlN layers in the superlattice, and the second one is related with periodic interruptions in the growth of superlattice for the evaporation of excess Ga metal. The dependences of the positions and intensities of the lines in the Raman spectra on the period of the superlattice are determined, and microscopic nature of optical phonon modes is established. The doublet structure of the $E(\text{TO})$ lines localized in the GaN and AlN layers of superlattice, genetically related to the $E_2(\text{high})$ and E_1 phonon branches of the bulk crystal, is first discovered and explained. A strong dependence of the polar modes localized in the AlN layer on the thickness of layer forming the superlattice is revealed. The results of complex studies will improve the accuracy of quantitative estimation of important parameters of superlattice structures and can be used to optimize growth parameters for the fabrication of structurally perfect short-period GaN/AlN superlattices.

1. Introduction

The great scientific interest in low-dimensional epitaxial heterostructures based on wide-gap A3-nitride compounds (Al,Ga)N is due to the unique possibility of creating optoelectronic devices operating both in the mid-ultraviolet and infrared-terahertz spectral ranges [1,2]. Such devices are promising for applications in multi-range spectroscopy, for the development of photodiagnostics and phototherapy methods in medicine, for the implementation of indirect optical communication systems, etc. Among the most important elements of such devices are short-period superlattices (SLs), with the thicknesses of the constituent layers varying from one to several monolayers (ML), i.e the $(\text{GaN})_m/(\text{AlN})_n$ SLs, where m and n are the numbers of GaN and AlN layers, respectively, in units of MLs (1ML=0.25nm). The most important requirements for such SLs are the presence of atomically smooth and homogeneous surfaces of the constituent layers and the extremely sharp interfaces. The solution of these problems requires a detailed study of the fundamental physical properties of SLs as well as the development of new methods for the quantitative diagnostics of their parameters with atomic resolution.

This article presents the results of studies related to the identification of physical mechanisms that determine structural and dynamic properties of short-period GaN/AlN SLs. Research is aimed at



developing scientifically based recommendations for optimizing the growth technology of high-quality epitaxial heterostructures.

2. Results and discussion

2.1. Growth

GaN/AlN SLs were grown on annealed and nitrated $c\text{-Al}_2\text{O}_3$ substrates using plasma-assisted molecular beam epitaxy (PA MBE) setup Compact 21T (Riber) equipped with a N_2 plasma source HD-25 (Oxford Appl.Res.), as described in detail in [3]. Briefly, the growth of AlN buffer layers was initiated by means of migration-enhanced epitaxy of the 65-nm-thick nucleation layer at the substrate temperature of 780°C followed by growth of the upper AlN buffer layer 210 nm thick using metal-modulated epitaxy at the same substrate temperature. The two-stage growth processes of these layers were started under slightly Me-enriched conditions with the ratio of Al and the activated nitrogen fluxes $\text{Al}/\text{N}_2^*=1.1$, which was changed to $\text{Al}/\text{N}_2^*=1.3$ in order to grow the last tens of nanometers of this layer with an atomically smooth surface morphology [4].

The growth runs of all short-period SLs $N \times \{\text{GaN}_m/\text{AlN}_n\}$, where N is the number of periods, were carried out at a constant substrate temperature of 690°C using slightly metal-rich conditions with ratios of metals (Ga,Al) and plasma activated nitrogen (N_2^*) fluxes of $\text{Ga}/\text{N}_2^*=1.70 \pm 0.05 \text{ ML/s}$ and $\text{Al}/\text{N}_2^*=1.02 \pm 0.02 \text{ ML/s}$. Therefore, the excess of Ga accumulated during the growth of GaN quantum wells could not be incorporated during the growth of AlN barrier layers, and the growth rates of these layers were controlled only by $\text{N}_2^*=0.50 \text{ ML/s}$. Periodic interruptions in the growth of SLs for 60 s after every 15–30 nm of their thickness were used to consume excess free metal atoms on the surface under a nitrogen flux. The substrates rotated with a constant speed of 30 rpm. The growth rate and surface morphology of the growing layers and SLs were controlled *in situ* using laser interferometry ($\lambda=532\text{nm}$) and reflected high energy diffraction (RHEED), respectively.

2.2 X-ray measurements

SLs were studied using high-resolution X-ray diffractometer D8DISCOVER, Bruker AXS. An analysis of the X-ray data made it possible to determine the period of the grown SLs and the ratio between the thicknesses of their constituent layers [5].

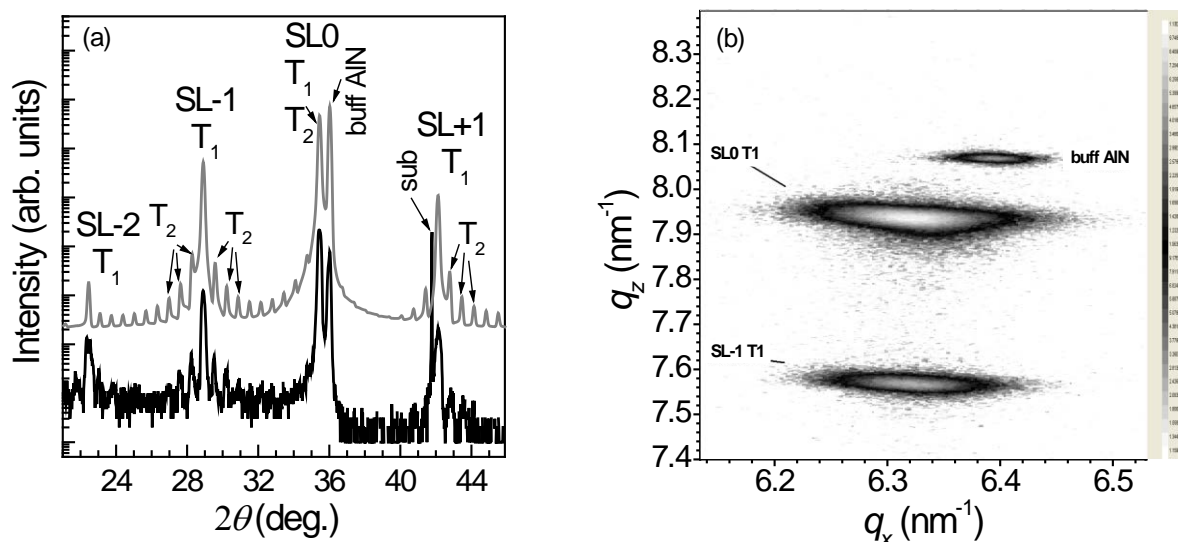


Figure 1. (a) Experimental (black) and modeled (gray) diffraction patterns obtained on the $(\text{GaN})_2/(\text{AlN})_4$ SL. The patterns are vertically shifted for convenience. (b) Example of an X-ray reciprocal space map for asymmetric reflection $(11\bar{2}4)$ from the $(\text{GaN})_6/(\text{AlN})_6$ SL.

X-ray diffractometry showed that the SLs have a double periodicity (figure 1). The first type of periodicity is formed by a sequence of bilayers, the thickness of which (T_1) is the sum of the $(\text{GaN})_m$ and $(\text{AlN})_n$ layers. The second type is characterized by $T_2=T_1 \cdot x + \Delta$, where Δ is the thickness of the additional GaN layer, formed during periodic interruptions in the growth of SLs to remove metallic atoms, x is the number of bilayer replications, T_1 is the thickness of the bilayer. The quantity Δ is comparable with the thickness of the GaN monolayer. It remains the same throughout the entire depth of the SL within the limits of measurement accuracy.

It was found that all the investigated short-period SLs completely relax at the boundary with the buffer, regardless of the number of GaN (m) and AlN (n) monolayers. Moreover, the layers which form SLs grow completely pseudomorphic with respect to each other. It is clearly seen from the reciprocal space map (figure 1b) that the centers of the spots of the scattering maxima (T_1) related to the SL are located under each other. Therefore, the parameter of the crystalline cell parallel to the surface (a_{\parallel}) does not change. The spot related to the AlN buffer is shifted toward lower a_{\parallel} values. The observed picture indicates the relaxation of the lattice relative to the buffer [5]. It has been established that SLs with a larger thickness of the AlN layer in the bilayer are characterised by the best structural perfection in the studied series of SLs.

2.3 *Ab initio* calculations

The *ab initio* calculations using plane-wave pseudopotential method were carried out within the local density approximation (LDA) provided by the Perdew and Wang functional parameterization [6] and generalized gradient approximation (GGA) with the Perdew-Burke-Ernzerhof exchange-correlation functional optimized for solids (PBEsol) [7] to density functional theory (DFT) as realized in ABINIT software package [8–10]. The fully nonlocal two-projector norm-conserving pseudopotentials used in the calculations were generated using the method suggested by Hamman [11]. For LDA calculations, the $3s3p$ electrons of Al atoms, the $2s2p$ electrons of N atoms, and the $3d4s4p$ electrons of Ga atoms were considered as the valence ones. In GGA calculations additional semi-core states were taken into account, namely $2s2p$ for Al and $3s3p$ for Ga atoms, increasing valence space of metal atoms. The test on convergence reveals that the energy cutoff of 45 Ha and the Brillouin zone (BZ) sampling as $6 \times 6 \times 4$ according to the Monkhorst-Pack scheme [12] is sufficient for high accuracy calculations. Full geometry optimization was performed by varying both the parameters of the cell and the positions of atoms in the unit cell. The convergence tolerance for geometry optimization was selected within 10^{-5} Ha/Bohr and 0.01 GPa in maximal force and stress tensor, correspondingly. The phonon wave vectors and frequencies were obtained in Γ -point of the BZ within the density functional perturbation theory (DFPT) [13,14]. The Raman spectra were simulated from the Raman tensor whose components are the third-order total-energy derivatives (with respect to the electric field and the atomic displacements) calculated within perturbation theory by applying the $(2n+1)$ theorem [15].

2.4 Raman measurements

The Raman measurements were performed at room temperature using a T64000 (Horiba Jobin-Yvon) spectrometer equipped with a confocal microscope. The line at 532 nm (2.33 eV) of Nd:YAG laser (Torus, Laser Quantum, Inc.) was used as the excitation source. All spectra were measured in a backscattering geometry. The scattering geometries are given in Porto notation, for example, $z(xx)\bar{z}$. Here, z is the direction of the 3-fold optical axis, and x and y are mutually orthogonal axes, which are arbitrarily oriented in the substrate plane.

The Raman spectra of $(\text{GaN})_m/(\text{AlN})_n$ SLs ($m=2,4,6$; $n=4,6$) were obtained both experimentally and theoretically. For better interpretation, the spectra in the region of optical phonon modes can be derived into two ranges, namely the mid-frequency range [560–680 cm^{-1}] and the high-frequency one [700–900 cm^{-1}]. The $E(\text{TO})$ modes are located in the mid-frequency range, while $A_1(\text{LO})$ modes are located in high-frequency range.

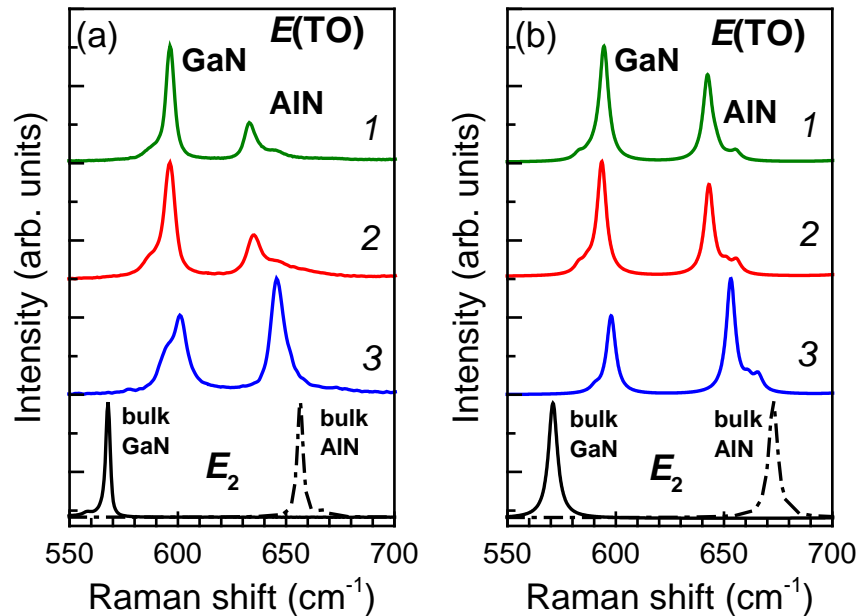


Figure 2. Experimental (a) and calculated (b) Raman spectra of (GaN)/(AlN) SLs in $z(xx)\bar{z}$ scattering geometry in the region of $E(TO)$ modes. Green (1), red (2) and blue (3) curves correspond to $(\text{GaN})_6(\text{AlN})_6$, $(\text{GaN})_4(\text{AlN})_4$, and $(\text{GaN})_2(\text{AlN})_4$ SLs, respectively. Black curves show the spectra of GaN (solid curve) and AlN (dash dotted curve) bulk crystals.

In contrast to the single lines for the $E(TO)$ symmetry modes observed in spectra of SL's with similar parameters grown by the MOCVD method [16], in the experimental spectra shown in figure 2a, the bands with an explicit doublet structure are observed. A similar doublet structure of the bands in the calculated spectra shown in figure 2b is also visible. A good agreement between experiment and theory is found, which made it possible to establish unambiguously a relationship between the features observed in the Raman spectra and the displacement patterns of the phonon modes. As an example, the atomic displacement patterns of $E(TO)$ modes in the $(\text{GaN})_4/(\text{AlN})_4$ SL are plotted in figure 3.

An analysis of the calculated eigenvectors of $E(TO)$ vibrational modes brings to conclusion that the both lines in the doublets correspond to phonons that are localized in GaN or AlN layers of SL. For

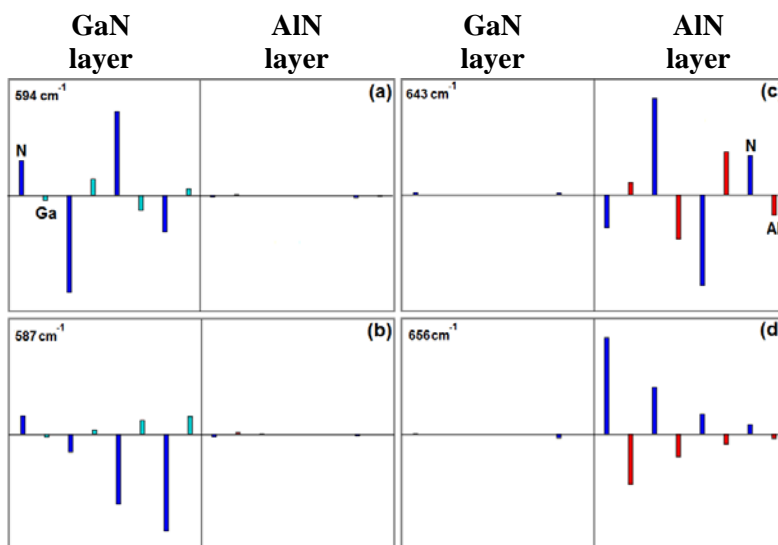


Figure 3. Atomic displacements for the high (a,c) and low (b,d) intensity modes $E(\text{GaN})$ (left column) and $E(\text{AlN})$ (right column) in $(\text{GaN})_4(\text{AlN})_4$ SL.

Table 1. The estimated values of strain (ε_{xx}) in GaN and AlN layers forming GaN/AlN SLs.

Layers	(GaN) ₂ /(AlN) ₄	(GaN) ₄ /(AlN) ₄	(GaN) ₆ /(AlN) ₆
GaN	$-1.53 \cdot 10^{-2}$	$-1.30 \cdot 10^{-2}$	$-1.32 \cdot 10^{-2}$
AlN	$+0.42 \cdot 10^{-2}$	$+0.78 \cdot 10^{-2}$	$+0.86 \cdot 10^{-2}$

localized phonon modes, their position in the Raman spectrum depends only on the individual characteristics of the layers and can be used, for example, to estimate the strain and its type (compression or tension). Using the data on the deformation potential constants for $E_2(\text{high})$ modes in bulk GaN and AlN crystals [17,18], we can estimate the sign and magnitude of the strains in the GaN and AlN layers forming the GaN/AlN SL. As follows from the analysis of the data presented in figure 2, planar strains ε_{xx} in the GaN and AlN layers have a compression and tensile character, respectively. Moreover, estimates show that the absolute value of the strain in GaN layers is greater than in AlN layers (see table 1). It has been established that the $E(\text{TO})$ modes have the localized nature which is retained even in the SL with the thinnest constituent layers, i.e. for (GaN)₂(AlN)₄. The high sensitivity of $E(\text{TO})$ phonons to the presence of strain is favorable factor for estimating this parameter in SL by Raman spectroscopy.

The appearance of doublets in the mid- and high frequency (560–900 cm^{-1}) range of Raman spectra can be explained based on the results of the group theoretical analysis. All optical modes of the short-period SLs can be classified according to their genesis from the modes of the constituent bulk (GaN and AlN) crystals based on the relation between the symmetry of the bulk crystals with the $P6_3mc$ (#186) space group and the symmetry of SL studied ($m+n = 2k$) with the $P3m1$ (#156) space group.

The SL optical modes originate from the two pairs of phonon bulk branches:

- 1) $\Gamma_1 - A_1$ ($A_1(\text{LO})$ -branch) and $\Gamma_4 - A_4$ (B_1 -silent branch)
- 2) $\Gamma_5 - A_5$ ($E_2(\text{TO})$ -branch) and $\Gamma_6 - A_6$ (E_1 -branch).

The very important symmetry property of each pair of branches is that they stick together at the A -point of the BZ, i.e. the form two pairs of complex-conjugated irreps $A_1 + A_4$ and $A_5 + A_6$ which

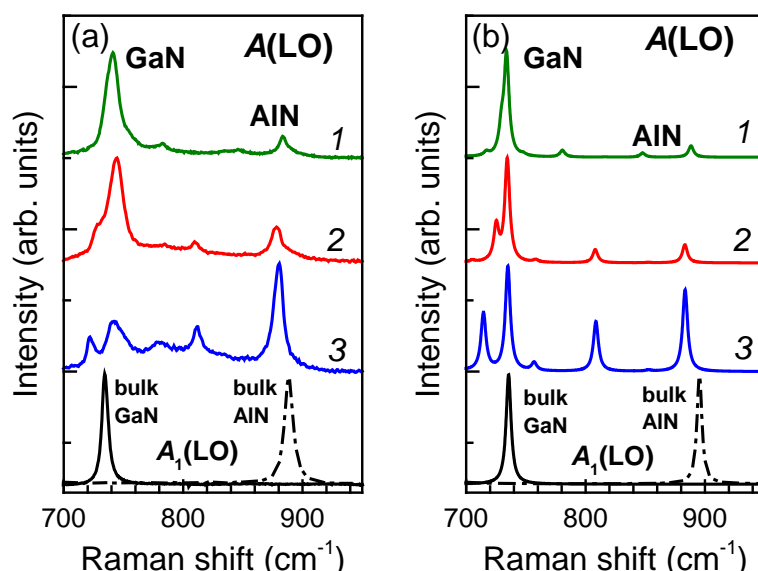


Figure 4. Experimental (a) and calculated (b) Raman spectra of (GaN)/AlN SLs in $z(xx)\bar{z}$ scattering geometry in the region of $A(\text{LO})$ modes. Green (1), red (2) and blue (3) curves corresponds to (GaN)₆(AlN)₆, (GaN)₄(AlN)₄, and (GaN)₂(AlN)₄ respectively. Black curves show the spectra of GaN (solid curve) and AlN (dash dotted curve) bulk crystals with low concentration of free carries.

correspond to two degenerate phonon states [20]. In SLs, this degeneracy is lifted due to the lowering of space symmetry from $P6_3mc$ (# 186) to $P3m1$ (# 156). As a result, each degenerate state at the A-point splits and then transforms into the Γ -states of the SL due to folding: $A_1 \rightarrow \Gamma_1$, $A_4 \rightarrow \Gamma_1$, and $A_5 \rightarrow \Gamma_3$, $A_6 \rightarrow \Gamma_3$. As a result, the small splitting of the degenerate bulk states at the BZ boundary leads to the formation of doublets at the Γ -point in SLs. The spectral line connected with the folded $A_1(\text{LO})$ -branch should be the most intense one in the doublet whereas the line genetically originated from B_1 -silent branch would have much lower intensity.

The high-frequency range of Raman spectra obtained in $z(xx)\bar{z}$ scattering geometry contains $A(\text{LO})$ phonons. The most intense bands in the range of $700\text{--}750\text{ cm}^{-1}$ are related to quasi-localized phonons in GaN layers. The atomic displacements are shown in figure 5a,b. The line in the Raman spectra with the highest frequency of $\sim 880\text{ cm}^{-1}$ is due to the mode localized in AlN layers. The atomic displacements related to this mode are plotted in the figure 5e. As seen from Raman spectra for $(\text{GaN})_m/(\text{AlN})_n$ ($m=2,4,6$; $n=4,6$) SLs (see figure 4), the intensity of the band increases with increasing of the AlN content in the SL. Among the high intensity peaks two low intensity peaks were found in the Raman spectra of $(\text{GaN})_4/(\text{AlN})_4$ SL in the range of $750\text{--}850\text{ cm}^{-1}$. The atomic displacement patterns of these modes are plotted in the figure 5c,d. The analysis of atomic displacements leads to conclusion that one of them with the lowest frequency is a delocalized mode (genesis of the mode is a mixture of silent B_1 - and $A_1(\text{LO})$ branches folded from the A-point at the BZ boundary) and the second one is localized in AlN layers of SL. The last mode is genetically originated from the $A_1(\text{LO})$ -branch of the bulk AlN crystal folded from the A-point the BZ boundary.

In addition, the analysis of the modes in all studied SLs showed that all modes with frequencies above 770 cm^{-1} are localized in AlN layers, and the Raman scattering intensity of these modes is related approximately as 1:2 to the intensity of the longitudinal mode $A(\text{LO})$ with the highest frequency. Following conception of the Brillouin zone folding which explains the number of phonons in SLs, the number of such modes grows linearly with increasing of SLs thickness. For example in case of $(\text{GaN})_4/(\text{AlN})_4$ SL there is only one band in Raman spectra in range $750\text{--}860\text{ cm}^{-1}$, while for $(\text{GaN})_4/(\text{AlN})_4$ SL there are two bands. It is noteworthy that the intensity of bands in Raman spectra

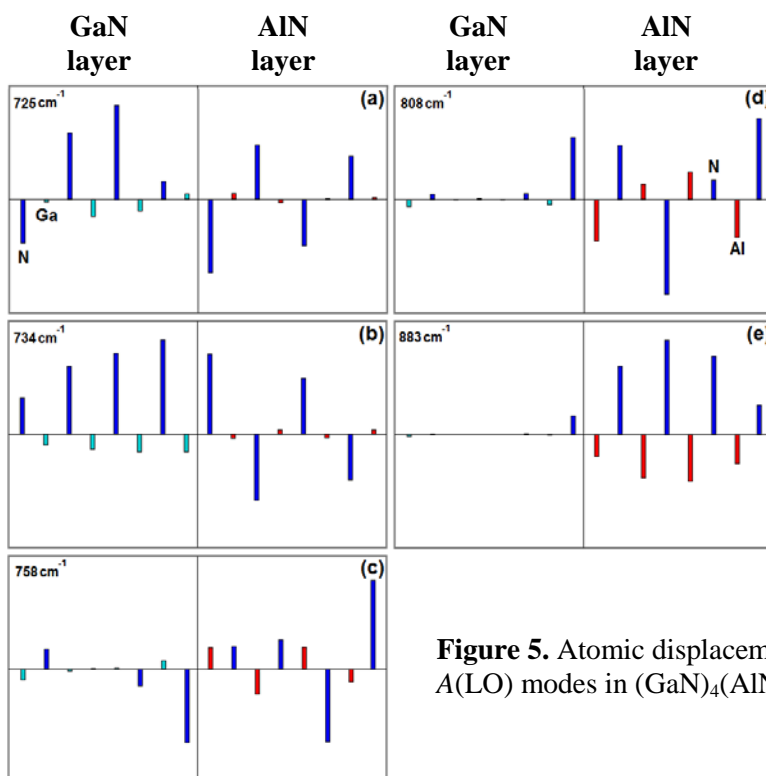


Figure 5. Atomic displacements for the $A(\text{LO})$ modes in $(\text{GaN})_4/(\text{AlN})_4$ SL.

related to localized modes in AlN layer increase significantly with increasing the AlN content in SLs with respect to GaN one. Such effects could be used to characterize the grown structure.

2.5 Electronic structure

The density functional theory suffers from systematic underestimation of the bandgap due to derivative discontinuity of the exchange-correlation energy [19]. Recently the number of advanced theoretical methods is developed in order to improve accuracy of the band structure predictions, for example hybrid functional method [20], or many-body perturbation theory [21]. The cost of such methods is strong computational demands, especially for crystal structures with tens of atoms in the unit cell. Alternatively the semi-empirical meta-GGA method taking into account kinetic energy of particles in exchange part of the functional [22] was found as a very cheap and accurate solution for band gap calculation problem. It was found that using semicore states, namely $2s2p$ for Al atom and $3s3p3d$ for Ga atom significantly increase accuracy of calculations. The table 2 reports on calculated band gap values for bulk wurzite nitrides and SLs $(\text{GaN})_m/(\text{AlN})_n$ ($m=2,4,6$; $n=4,6$) calculated using GGA and meta-GGA (mGGA) approximations. Comparing the calculated values for bulk crystals with experimental data, we found a very good accuracy of the mGGA approximation and a strong underestimation of the GGA, however it should be noted that the tendency towards a decrease in the band gap value with an increase in the SL period is the same for both approximations.

Table 2. Calculated band gap values (in units of eV).

Compound	Exp	GGA	mGGA
GaN	3.47	1.91	3.67
AlN	6.12	4.12	6.05
$(\text{GaN})_2/(\text{AlN})_4$	–	2.88	4.60
$(\text{GaN})_4/(\text{AlN})_4$	–	2.46	4.06
$(\text{GaN})_6/(\text{AlN})_6$	–	2.14	3.88

It follows from Table 2 that the value of band gap decreases with an increase in the layer thickness in the case of the SLs $(\text{GaN})_m/(\text{AlN})_n$ with the equal thickness of the constituent layers of GaN and AlN ($m=n$) and increases with increasing AlN content relative to GaN ($n>m$). Such dependence opens the gate to construction of the SL with given band gap.

3. Summary and conclusion

The structural and dynamic properties of short-period GaN/AlN SLs grown by the submonolayer digital PA MBE method were studied. Analysis of the high-resolution X-ray diffraction data allowed us to determine the period of the grown SLs and the ratio between the thicknesses of their constituent layers. It was found that two types of interfaces exist in the grown samples. One type is associated with a periodic sequence of GaN and AlN layers in the SLs and the other one is associated with periodic interruptions in the growth of SLs during the process of digital epitaxy for the evaporation of excess Ga-metal. Experimentally, the dynamic properties of the crystal lattice of SLs were studied by Raman spectroscopy. The spectra were interpreted using *ab initio* calculations of nonlinear optical properties in the framework of the density functional theory, aimed at studying the phonon states of SLs. The calculations were performed for SLs with both equal and unequal layer thicknesses. As a result, the phonon mode frequencies were calculated and the atomic displacement patterns were established. This led to the conclusion on the microscopic nature of the vibrational modes of the SLs.

The dependences of the positions and intensities of the lines in the Raman spectra on the period of the SL are determined and a symmetry relationship was established between the vibrations of the bulk GaN(AlN) crystal and the SL at the symmetry points of the Brillouin zone. The doublet structure of the $E(\text{TO})$ lines localized in the GaN and AlN SL layers genetically related to the $E_2(\text{high})$ - and E_1 -

branches of the bulk crystal was first discovered and explained. The results will improve the accuracy of the quantitative estimation on the base of Raman data of strain in the individual layers forming the SL. In the high-frequency region of the spectrum, the maximum response was obtained from the polar $A_1(\text{LO})$ -branch folded from the A-point at the BZ boundary accompanied by a weak satellite from the silent B_1 -branch also folded from the A-point. The calculations revealed a strong dependence of the polar modes localized in AlN layers on the thickness of layers forming the SL. The greater the AlN layer thickness, the greater the Raman intensity of the phonon localized in this layer and *vice versa*. The results of the comprehensive studies can be successfully used to optimize the parameters of the growth process in order to form structurally perfect short-period GaN/AlN SLs.

Experimental studies of the electronic structure of short-period GaN/AlN SLs are carried out by low-temperature photoluminescence measurements. The results of the studies will be presented in a separate paper.

Acknowledgments

The work was supported in part by Russian Foundation for Basic Research (project RFBR-BRICS №17-52-80089). XRD characterizations were performed using equipment of the Federal Joint Research Center “Material science and characterisation in advanced technology” sponsored by the Ministry of Education and Science of the Russian Federation.

References

- [1] Lim C B, Ajay A, Lähnemann J, Browne D A and Monroy E 2017 III-nitride nanostructures for intersubband optoelectronics *III-Nitride Materials, Devices and Nano-Structures* (World Scientific Publishing Europe Ltd) chapter 3 pp 77–113
- [2] Beeler M, Trichas E and Monroy E 2013 *Semicond. Sci. Technol.* **28** 074022
- [3] Jmerik V N, Nechaev D V and Ivanov S V 2018 *Molecular Beam Epitaxy (MBE): From Research to Mass Production, 2nd Edition*, ed. by M.Henini, (Amsterdam: Elsevier) chapter 8 pp 135–179
- [4] Nechaev D V, Koshelev O A, Ratnikov V V, Brunkov P N, Myasoedov A V, Sitnikova A A, Ivanov S V and Jmerik V N 2020 *Superlattices and Microstructures* **138** 106368
- [5] Pietsch U, Holy V, Baumbach T 2004 *High-Resolution X-Ray Scattering, 2nd Edition* (New York: Springer-Verlag) part III, chapter 9 pp.179–192 part IV chapter 13 pp 317–329
- [6] Perdew J and Wang Y 1992 *Phys. Rev. B* **45** 13244–9
- [7] Perdew J, Ruzsinszky A, Csonka G et al. 2009 *Phys. Rev. Lett.* **100** 136406
- [8] Gonze X, Beuken J-M, Caracas R et al. 2002 *Comput. Mater. Sci.* **25** 478–92
- [9] Gonze X, Rignanese G, Verstraete M et al. 2005 *Z. Kristallogr.* **220** 558–62
- [10] Gonze X, Amadon B, Anglade P-M et al. 2009 *Comput. Phys. Commun.* **180** 2582–615
- [11] Hamann D R 2013 *Phys. Rev. B* **88** 085117
- [12] Monkhorst H J and Pack J D 1976 *Phys. Rev. B* **13** 5188–92
- [13] Gonze X 1997 *Phys. Rev. B* **55** 10337–54
- [14] Gonze X and Lee C 1997 *Phys. Rev. B* **55** 10355–67
- [15] Gonze X and Vigneron J-P 1989 *Phys. Rev. B* **39** 13120–8
- [16] Davydov V Yu, Roginskii E M, Smirnov A N, Kitaev Yu E, Yagovkina M A, Kyutt R N, Rozhavskaia M M, Zavarin E E, Lundin W V and Smirnov M B 2013 *Phys. Status Solidi A* **210** 484–7
- [17] Davydov V Yu, Averkiev N S, Goncharuk I N, Nelson D K, Nikitina I P, Polkovnikov A S, Smirnov A N, Jacobson M A and Semchinova O K 1997 *J. Appl. Phys.* **82** 5097–102
- [18] Sarua A, Kuball M and Van Nostrand J E 2002 *Appl. Phys. Lett.* **81** 1426–8
- [19] Perdew J 1985 *Int. J. Quantum Chem.* **28** 497–523
- [20] Becke A J. 1993 *Chem. Phys.* **98** 1372–7
- [21] Shishkin M and Kresse G 2007 *Phys. Rev. B* **75** 235102
- [22] Tran F and Blaha P 2009 *Phys. Rev. Lett.* **102** 226401